

Revisiting the Friedel Sum Rule for single channel quantum wire

Swarnali Bandopadhyay and P. Singha Deo

S.N. Bose National Centre for Basic Sciences, J.D.Block, Sector III, Salt Lake City, Calcutta 700098, India
(February 17, 2019)

Elastic scattering in a quantum wire has several novel features not seen in 1D, 2D or 3D. In this work we consider a single channel quantum wire as its application is inevitable in making devices based on quantum interference effects. We consider a point defect or a single delta function impurity in such a wire and show how some of these novel features affect Friedel-sum-rule (FSR) in a way, that is quite unlike in 1D, 2D and 3D.

PACS: 73.23.-b, 72.10.-d, 72.10.Bg

I. INTRODUCTION

The density of states in a mesoscopic sample and its relation to the scattering matrix is very important to understand mesoscopic transport phenomena. Therein it is believed that the transport across a mesoscopic sample can be formalized in terms of the scattering matrix. The mesoscopic sample is considered as an elastic scatterer, couple to electron reservoirs (that act like batteries) through ideal leads. The frequency dependent response, the degree of dephasing and several other physical quantities in such a mesoscopic sample depend directly or indirectly on the density of states [1]. The Friedel-sum-rule (FSR) relates the density of states (DOS) to the scattering matrix and can be stated as [2]

$$\theta_f(E_2) - \theta_f(E_1) \approx \pi N(E_2, E_1) . \quad (1)$$

In 1D, 2D and 3D, the equality being approximate is almost exact in the WKB regime where generally transport occurs. Here $N(E_2, E_1)$ is the variation in the number of states in the energy interval $[E_1, E_2]$ due to the scatterer and [3]

$$\theta_f(E) = \frac{1}{2} \sum_j \xi_j = \frac{1}{2i} \ln(\det[S]) . \quad (2)$$

S is the scattering matrix corresponding to a scattering phenomenon and $e^{i\xi_j}$, $j=1,2,\dots,n$ are the n eigenvalues of the unitary matrix S . In differential form the FSR can also be stated as

$$\frac{\partial}{\partial E} \theta_f(E) = \frac{1}{2i} \frac{\partial}{\partial E} \ln(\det[S]) \approx \pi [\rho(E) - \rho_0(E)] , \quad (3)$$

where $[\rho(E) - \rho_0(E)]$ is the variation of the DOS or the difference in the DOS due to the presence of the scatterer. $\rho(E)$ and $\rho_0(E)$ can be found by integrating the local DOS (LDOS) $\rho(x, y, z, E)$ and $\rho_0(x, y, z, E)$ which are related to the electron probabilities.

Ref. [1] explores a relation between LDOS and the scattering matrix. In that case the oscillating part of LDOS that originates from quantum interference effects, poses a problem [4], but never the less there could be an exact relation that connects the LDOS to the scattering matrix [1]. However, if one wants to integrate the LDOS to

find the DOS, then it is very cumbersome as compared to Eq. (1) and Eq. (3). Besides, in this local formalism, one has to take the derivatives of the S matrix elements with respect to the local potential and in some cases one encounters problems in including the non-local effects and non-local disturbances in the DOS. In this work we intend to study the Friedel sum rule (Eq. (1) and Eq. (3)) for a single channel quantum wire with a delta-function impurity.

The scattering matrix of an impurity in a quantum wire have very unusual features that were not realized until very recently [5,6]. In this respect the single channel quantum wire is quite distinct from multichannel ones [7]. A single channel quantum wire has a 2×2 scattering matrix. In the presence of a single attractive impurity, taken as a negative delta-function potential, the transmission probability can go to zero [5] for some finite energy of the incident electron. At the corresponding energy, the scattering phase-shift shows a discontinuous jump(slip) by π [6]. It was shown that in the single channel case the Friedel phase θ_f is not affected by the discontinuous phase drops [8,9].

In the multichannel case, when the unitarity of a particular channel is not present and the electron can escape to a different channel, the transmission zeroes are replaced by minimas and the discontinuous phase slip by π are replaced by continuous and less than π phase drops [7]. Subsequently it was also shown that in the multi channel case too the Friedel phase θ_f is not affected by these continuous phase drops [7]. However, $\frac{\partial \theta_f(E)}{\partial E}$ may not bear any resemblance to $\pi [\rho(E) - \rho_0(E)]$ [7].

In this work we come back to the single channel quantum wire with a point defect or a delta function potential and show that the peculiarities of electron propagation in such a system is so diverse that the FSR, sometimes does not hold good even in the WKB regime and sometimes hold good in non-WKB regime. Thus in view of the recent importance that scattering phase shifts have gained with respect to transport in mesoscopic systems and the unknown features of single channel quantum wires, in this paper we revisit the FSR in single channel Q1D quantum wire. The single channel case being the most important because it is in this regime that one can really control the quantum interference effects and use them to build

mesoscopic devices [10].

II. DERIVATION OF FRIEDEL SUM RULE

In this section we shall briefly review the outline of the derivation of FSR. Scattering due to a spherical defect (within an approximation this can also be taken for non-spherical defects) leads to asymptotic wave-functions that are plane waves and whose radial part is of the form [11]

$$\psi_{k,l}(r) \sim \frac{1}{r} \sin(kr - \frac{l\pi}{2} + \eta_l) . \quad (4)$$

Here, k is the wave-number, l is the angular momentum quantum number and η_l is the phase shift due to scattering. According to Friedel, an approximate way to count the number of states created by the impurity is the following [11]. Consider a large sphere of radius R with a defect at the centre. Generally, scattering states have open boundary conditions that lead to their characterization in terms of complex energies. The imaginary part of their complex energy is called self energy and it arises because of the fact that the states can leak out to infinity and get absorbed by some detector there irrespective of boundary conditions. In a 1D scattering problem, interaction of the states with semi-infinite leads give rise to this self energy [10]. In this case also the interaction of the states within the large sphere of radius R with the region outside the sphere will lead to a self energy. Neglecting the contribution due to self-energy we impose a condition

$$\psi_{k,l}(r) = 0 \quad \text{at } r = R. \quad (5)$$

This should not be mistaken as Dirichlet boundary condition. This is an intuitive method for counting states and error can be there due to neglecting the self energy. Thus we obtain from Eq. (4)

$$kR - \frac{l\pi}{2} + \eta_l = n\pi . \quad (6)$$

The states k given by Eq. (6) are real and not complex as it should be in the case of scattering states with a finite self energy. In absence of the scatterer, the scattering phase shift $\eta_l = 0$ and

$$kR - \frac{l\pi}{2} = m\pi \quad (7)$$

Eq. (6) and Eq. (7) give the number of allowed values of k (the number of states associated with resonances to be more precise) in presence and absence of the scatterer. Thus it follows that the number of new states (due to new resonant states) created by the defect in the range k' to k is [11]

$$\frac{\eta_l(k) - \eta_l(k')}{\pi}.$$

A more rigorous derivation, including the self energy is given in Ref. [12].

$$\frac{\partial}{\partial E} \theta_f(E) = \text{Im} \text{Tr} \left[\hat{G}^a \left(1 - \frac{\partial \hat{\Sigma}^a}{\partial E} \right) \right] . \quad (8)$$

$$\text{Here } \hat{G}^a = \left[E - \hat{H}_{\text{system}} - \hat{\Sigma}^a(E) \right]^{-1} , \quad (9)$$

is the advanced Green's function and $\hat{\Sigma}^a$ is the corresponding self energy. Thus

$$\begin{aligned} \frac{\partial}{\partial E} \theta_f(E) + \text{Im} \text{Tr} \hat{G}^a \frac{\partial \hat{\Sigma}^a}{\partial E} &= \text{Im} \text{Tr} \hat{G}^a \\ &= \pi [\rho(E) - \rho_0(E)] . \end{aligned} \quad (10)$$

Note that \hat{G}^a is the advanced Greens function for the system alone, where the modifications in the system due to the presence of the leads is included. Hence apart from this $\text{Im} \text{Tr} \hat{G}^a$ which is equal to the integrated disturbance in the LDOS created by the impurity, i.e., $\pi[\rho(E) - \rho_0(E)]$, there will be some disturbance in the LDOS in the leads which will depend on the Greens function of the lead and how it is affected by the system. This contribution is not important and also it gets screened away very easily as it is very small and the leads being ideal, carrier concentration is very high in the leads (this is often referred to as non-polarizable leads). So $\rho(E) - \rho_0(E)$ in Eq. (10) is the integrated LDOS and the LDOS is peaked at the impurity site, decaying away from the impurity site all the way upto $\pm\infty$. The only assumption required to get Eq.(3) is to neglect $\frac{\partial \hat{\Sigma}^a}{\partial E}$ i.e. the energy dependence of the self energy. Now [10]

$$\frac{\partial}{\partial E} \hat{\Sigma}^a = \frac{\partial}{\partial E} [\tau_p g_p^a \tau_p^\dagger] , \quad (11)$$

where, g_p^a is the local Green's functions of the semi-infinite leads at the sample end and τ_p is the matrix element which couples the leads to the sample. In 1D, 2D and 3D it is easy to calculate the importance of the term thrown away. When using this Green's function approach in Q1D systems, the system is discretized so that the term in square bracket [] in equation (9) becomes a finite dimensional matrix and inverting it we can get the Green's function. While discretising the system we assume that the coupling between the sample and the leads are just parameters, independent of energy E . This is equivalent to saying τ_p & τ_p^\dagger in (11) are independent of energy. In 1D, 2D and 3D this is actually the case in the WKB regime. So in the WKB regime the only energy dependence of $\hat{\Sigma}^a$ can come from the energy dependence of g_p^a . g_p^a being the local Greens function of a semi-infinite ideal wire, its energy dependence is not very important. Thus in 1D, 2D and 3D, in the WKB regime, FSR [Eq.(1), (3)] is almost exact. It is worth

while to mention that transport normally occurs in this WKB regime and this is normally the regime of interest.

But quasi-1D is a new system and as discussed in the introduction, has several new features like discontinuous phase jumps and transmission zeroes. One should not take for granted, notions that are accepted in 1D, 2D and 3D. To make a quantitative analysis of how big are the terms that are thrown away we do not use the Green's function technique where τ_p & τ_p^\dagger are just parameters that are independent of energy, but use the first principle method of solving the Schrödinger equation in various regions and then do the mode matching at all energies.

III. FIRST PRINCIPLE CALCULATION OF SCATTERING MATRIX AND DOS IN Q1D QUANTUM WIRE

The Schrödinger equation in a Q1D quantum wire (shown in Fig.(1)) is

$$\left[-\frac{\hbar^2}{2m_e} \left(\frac{\partial^2}{\partial x^2} + \frac{\partial^2}{\partial y^2} \right) + V_c(y) + V_d(x, y) \right] \Psi(x, y) = E \Psi(x, y) \quad (12)$$

Here, $V_c(y)$ is the confinement potential along y -direction. We assume this potential as hard wall type, i.e.,

$$\begin{aligned} V_c(y) &= \infty & y \geq \left| \frac{W}{2} \right| \\ &= 0 & y < \left| \frac{W}{2} \right| \end{aligned} \quad (13)$$

$V_d(x, y)$ is the impurity potential at $(0, y_i)$ and we take

$$V_d(x, y) = \gamma \delta(x) \delta(y - y_i)$$

In y -direction the $\Psi(x, y)$ in Eq. (12) will obey the same boundary conditions as the $\chi_n(y)$ below,

$$\left[-\frac{\hbar^2}{2m_e} \frac{d^2}{dy^2} + V_c(y) \right] \chi_n(y) = E_n \chi_n(y), \quad (14)$$

which makes it possible to expand $\Psi(x, y)$ at a given x , in terms of the $\chi_n(y)$ s. Thus

$$\Psi(x, y) = \sum_n c_n(x) \chi_n(y) . \quad (15)$$

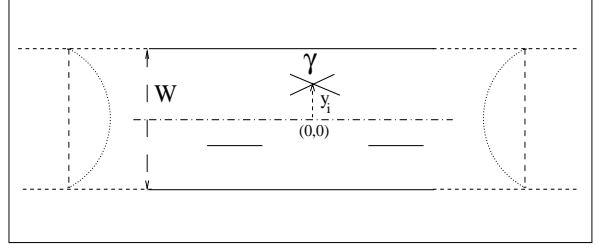


FIG. 1. Here we show a quantum wire of width W defined by the potential in Eq. (13). The dash-dotted curve is a line through the middle of the quantum wire, and it is also taken to be the x -axis. The origin of the coordinates is shown in the figure. An impurity delta function potential $V_d(x, y) = \gamma \delta(x) \delta(y - y_i)$ is situated at $x = 0$ and $y = y_i$ and marked as \times . We consider scattering effects when the incident electron is from the left with an energy E . In the energy range $\frac{\pi^2 \hbar^2}{2m_e W^2} < E < \frac{4\pi^2 \hbar^2}{2m_e W^2}$, there is only one transverse mode that propagates and the rest of the modes are evanescent. The impurity at \times mixes the different modes to give scattering matrix elements. The transverse wave function in the incident and transmitted channels is shown by dotted lines.

Substituting this in Eq. (12) we get

$$\frac{d^2 c_n(x)}{dx^2} + k_n^2 c_n(x) = \sum_m \Gamma_{nm}(x) c_m(x) \quad (16)$$

$$\text{where } k_n^2 = \frac{2m_e}{\hbar^2} (E - E_n) , \quad (17)$$

k_n being the wave vector. $E_n = \frac{n^2 \pi^2 \hbar^2}{2m_e W^2}$, where $n = \pm 1, \pm 2, \pm 3, \dots$ and

$$\Gamma_{nm}(x) = \frac{2m_e}{\hbar^2} \int \chi_n^*(y) V_d(x, y) \chi_m(y) dy . \quad (18)$$

Asymptotically ($x \rightarrow \pm\infty$) $V_d(x, y) = 0$, Γ_{nm} is also 0 and the solutions to Eq. (16) are

$$c_n(x) = \begin{cases} A_n e^{ik_n x} + B_n e^{-ik_n x}, & x < 0 \\ C_n e^{ik_n x} + D_n e^{-ik_n x}, & x > 0, \end{cases} \quad (19)$$

for the propagating modes ($E > E_n$ in Eq. (17)) and by setting $k_n = ik_n$, we obtain

$$c_n(x) = \begin{cases} A_n e^{-\kappa_n x} + B_n e^{\kappa_n x}, & x < 0 \\ C_n e^{-\kappa_n x} + D_n e^{\kappa_n x}, & x > 0, \end{cases} \quad (20)$$

for the evanescent modes ($E < E_n$ in Eq. (17)). Obviously $A_n = D_n = 0$ for the evanescent modes given in Eq.(20). To have the n -th mode to be propagating it is necessary that $k_n^2 > 0$ and the rest of the modes will be evanescent. In case of many propagating channels, for an electron incident from the left in Fig. (1) along the sub-band n , the amplitude of transmission to a channel m on the right is given by

$$\tilde{t}_{nm} = \left(\frac{k_m}{k_n} \right)^{\frac{1}{2}} t_{nm} = \left(\frac{k_m}{k_n} \right)^{\frac{1}{2}} \frac{C_m}{A_n} , \quad (21)$$

and the amplitude of reflection to a channel m on the left is given by

$$\tilde{r}_{nm} = \left(\frac{k_m}{k_n}\right)^{\frac{1}{2}} r_{nm} = \left(\frac{k_m}{k_n}\right)^{\frac{1}{2}} \frac{B_m}{A_n}. \quad (22)$$

n and m in Eq. (21) and Eq. (22) should be for propagating channels only.

As we consider single propagating channel, we have only one transmission amplitude \tilde{t}_{11} and one reflection amplitude \tilde{r}_{11} . Apart from these two unknown parameters there are ∞ unknown parameters that come from the evanescent modes in Eq. (20). To have a single propagating channel ($k_1^2 > 0$) we find from Eq. (17) that

$$\frac{\pi^2 \hbar^2}{2m_e W^2} < E < \frac{4\pi^2 \hbar^2}{2m_e W^2}. \quad (23)$$

The unknown parameters are to be determined by mode matching. After doing the mode matching one finds an infinite set of equations that can be written in matrix form as [5]

$$\begin{pmatrix} \Gamma_{11} - 2ik_1 & \Gamma_{12} & \Gamma_{13} & \dots \\ \Gamma_{21} & \Gamma_{22} + 2\kappa_2 & \Gamma_{23} & \dots \\ \Gamma_{31} & \Gamma_{32} & \Gamma_{33} + 2\kappa_3 & \dots \\ \Gamma_{41} & \Gamma_{42} & \Gamma_{43} & \dots \\ \dots & \dots & \dots & \dots \\ \dots & \dots & \dots & \dots \end{pmatrix} \begin{pmatrix} t_{11} \\ t_{12} \\ t_{13} \\ \vdots \end{pmatrix} = \begin{pmatrix} -2ik_1 \\ 0 \\ 0 \\ \vdots \\ \vdots \end{pmatrix}, \quad (24)$$

where, $\Gamma_{nm} = \frac{2m_e \gamma}{\hbar^2} \text{Sin}[\frac{2\pi}{w}(y_i + \frac{w}{2})] \text{Sin}[\frac{m\pi}{w}(y_i + \frac{w}{2})]$.

t_{11} is defined in Eq. (21) as $\frac{C_1}{A_1}$ and $t_{12} = \frac{C_2}{A_1}$, $t_{13} = \frac{C_3}{A_1}$ and so on. All the unknowns t_{11}, t_{12}, \dots can be determined by solving this matrix equation that involves inverting the infinite dimensional matrix on the L.H.S of Eq. (24). Once we know t_{11} we can find \tilde{t}_{11} . In practice, inverting the matrix is not necessary as Bagwell [5] has given a nice expression for \tilde{t}_{11} as

$$\tilde{t}_{11} = 1 + \frac{-i\frac{\Gamma_{11}}{2k_1}}{1 + \sum_{n>1} \frac{\Gamma_{nn}}{2\kappa_n} + i\frac{\Gamma_{11}}{2k_1}} \quad (25)$$

We find that such a similar expression exists for the other parameters too, given by

$$t_{1n} = \frac{-\frac{\Gamma_{1n}}{2\kappa_n}}{1 + \sum_{n>1} \frac{\Gamma_{nn}}{2\kappa_n} + i\frac{\Gamma_{11}}{2k_1}} \quad (26)$$

\tilde{r}_{11} can be obtained from the constraint of current conservation as

$$\tilde{t}_{11} = 1 + \tilde{r}_{11}. \quad (27)$$

The scattering matrix S for this single channel Q1D system is

$$S = \begin{pmatrix} \tilde{r}_{11} & \tilde{t}_{11} \\ \tilde{t}_{11} & \tilde{r}_{11} \end{pmatrix}. \quad (28)$$

These scattering matrix elements define the scattering properties of the impurity potential completely. When the impurity potential is positive it can only support scattering states. However when the impurity potential is negative, it can also support some bound states, apart from the scattering states. From Eq.(17) we see that for each n we get a sub-band of scattering states (E as a function of k_n). Similarly we get a bound state for each n . For $n=1$ the bound state energy is given by the solution to the following equation.

$$1 + \sum_{n=1}^{\infty} \frac{\Gamma_{nn}}{2\kappa_n} = 0 \quad , \quad (29)$$

and it is true bound state. For $n=2$ again the bound state energy is given by the solution to the following equation

$$1 + \sum_{n=2}^{\infty} \frac{\Gamma_{nn}}{2\kappa_n} = 0 \quad . \quad (30)$$

This bound state for $n=2$ may or may not be a true bound state. If the impurity potential is such that the solution to the Eq.(30) lie in the range given in Eq.(23), then this bound state for $n = 2$, is degenerate with $n=1$ scattering state and it becomes a quasi-bound state. The scattering matrix contains all informations of this quasi-bound state, and solving the scattering problem is sufficient. The DOS shows a sharp peak at the energy given by the solution to the Eq.(30). Even the true bound state can be understood from analytic continuation of the S -matrix.

General definition of the LDOS is

$$\rho(x, y, E) = \sum_{m, k_m} \delta(E - E_{m, k_m}) |\psi(x, y)|^2 \quad (31)$$

The incident electron wave-function is $A_m e^{ik_m x} \text{Sin}[\frac{m\pi}{W}(y + \frac{W}{2})]$, with energy $E_{m, k_m} = \frac{m^2 \pi^2 \hbar^2}{2m_e W^2} + \frac{\hbar^2 k_m^2}{2m_e}$, where we have taken that the electron is incident from the left i.e., $x < 0$. $\psi(x, y) = \sum_n c_n(x) \text{Sin}[\frac{n\pi}{W}(y + \frac{W}{2})]$ is electron wave function in the region of mode mixing as given in Eq. (15) for V_c defined in Eq.(13). Using this $\psi(x, y)$ from Eq. (31) we have calculated to find(see Appendix)

$$\begin{aligned} [\rho(E) - \rho_0(E)]_{total} &= \sum_m \frac{2|\tilde{r}_{mm}|}{hv_m} \int_{-\infty}^{\infty} dx \text{Cos}(2k_m x + \eta_m) \\ &+ \sum_m \frac{2}{hv_m} \sum_n \frac{|t_{mn}|^2}{\kappa_n}, \end{aligned} \quad (32)$$

\sum_m denotes sum over all propagating modes and \sum_n denotes sum over all evanescent modes. The 1st term on the R.H.S. is basically due to the change in the LDOS in the leads. One can see that this term gives an unimportant small contribution that does not change with energy in the WKB regime (as is evident that the integrand is an oscillatory function and the outcome of the integration will not depend much on the frequency of oscillation. Also one can see that this term is further weighted down by $|\tilde{r}_{mm}|$ which is negligibly small in the WKB regime wherein the particle is almost entirely transmitted and $\frac{\tilde{r}_{mm}}{v_m}$ is almost independent of energy). Also the carrier concentration in the leads is normally large enough to screen away a small oscillatory LDOS completely. So the relevant quantity that appears in FSR is

$$\rho(E) - \rho_0(E) = \sum_m \frac{2}{hv_m} \sum_n \frac{|t_{mn}|^2}{\kappa_n}, \quad (33)$$

where again sum over n is for the evanescent modes only. This is actually the integrated local DOS around the impurity site and decaying away from the impurity site all the way upto $\pm\infty$. This quantity ultimately determines the effects produced by the impurity and is very important. In the regime of single propagating channel we have

$$\rho(E) - \rho_0(E) = \frac{2}{hv_1} \sum_{n>1} \frac{|t_{1n}|^2}{\kappa_n}, \quad (34)$$

Thus we can independently calculate the both sides of Eq. (3) starting from the 1st principles, where we do not have to throw away dispersive behavior or energy dependence of self energy. In the next section we discuss the agreement and disagreement in detail keeping track of the energy dependent self energy as well as the oscillating LDOS in the leads. The later is just for completeness.

IV. RESULTS AND DISCUSSION

We would first like to discuss about what is the WKB regime for a quantum wire with a δ -function potential with a specific example (inset to Fig. 2). Normally when the incident electron does not feel the potential very strongly is taken to be the WKB regime [13]. In the inset of Fig.(2), where we plot $|\tilde{r}_{11}|^2$ versus incident energy we find that there are three regimes. One is to the left of point P_1 where $|\tilde{r}_{11}|^2$ is large and also strongly energy dependent. The other is between the points P_1 and Q_1 where $\frac{\hbar^2 k_1^2}{2m_e} \gg \gamma$. These two regimes can be seen in 1D scattering and are the non-WKB and WKB regimes respectively. The third regime is to the right of the point Q_1 , where again $|\tilde{r}_{11}|^2$ is very small and is hence a WKB regime, but the energy dependence of $|\tilde{r}_{11}|^2$ is very large. Such a regime cannot be seen in 1D and is a speciality of Q1D. So the energies that lie to the left of P_1 is where the electron feels the potential very strongly and is almost entirely reflected back and is the non-WKB regime.

Energies to the right of the point P_1 correspond to the WKB limit. The alternate definition that in the WKB regime the wavelength is much smaller than the scale at which the potential changes is meaningless in mesoscopic systems, because scattering comes not only from the potential but also from the boundary and several examples can be cited wherein the small wavelength behavior is identical to the large wavelength behavior [14].

In Fig.(2) we find a large deviation of $\pi[\rho(E) - \rho_0(E)]$ (dotted curve) from $\frac{d\theta_f}{dE}$ (solid curve) at energies in the non-WKB regime (left of P_1). This is similar to what is seen in 1D, 2D or 3D. In the WKB regime, that is to the right of the point P_1 , although $|\tilde{r}_{11}|^2$ is very small, its energy dependence is not as negligible as that of a potential in 1D (eg, a delta function potential in 1D or a square well in 1D). Energy dependence of $|\tilde{r}_{11}|^2$ automatically implies energy dependence of τ_p or dispersive behavior. So there is an appreciable difference between $\pi[\rho(E) - \rho_0(E)]$ and $\frac{d\theta_f}{dE}$. The difference is coming due to non negligible contribution of $\frac{d\hat{\Sigma}^a}{dE}$. More precisely $\frac{d}{dE} |\tau_p|^2$ is large (dispersive behavior), g_p^a being finite. Let us now analytically analyze the curves (solid and dashed) to the right of Q_1 . In this region $\kappa_2 = \sqrt{\frac{2m_e}{\hbar^2}(E_2 - E)} \rightarrow 0$. From Eq.(34) we find that only the 1st term in the series is relevant. That is

$$\pi[\rho(E) - \rho_0(E)]_{\kappa_2 \rightarrow 0} \text{ diverges as } \left[\frac{2\pi}{hv_1} \frac{\Gamma_{11}}{\Gamma_{22}} \frac{1}{\kappa_2} \right]_{\kappa_2 \rightarrow 0} \quad (35)$$

Similarly one can find

$$\left[\frac{d\theta_f}{dE} \right]_{\kappa_2 \rightarrow 0} = \left[\frac{d}{dE} \arg(\tilde{t}_{11}) \right]_{\kappa_2 \rightarrow 0} \quad (36)$$

$$\text{diverges as } \left[\frac{2\pi}{hv_1} \frac{\Gamma_{11}}{\Gamma_{22}} \frac{1}{\kappa_2} \right]_{\kappa_2 \rightarrow 0} \quad (37)$$

Note that although $\arg(\tilde{t}_{11})$ can have a discontinuity, the derivative exists at all energies. Essentially the right derivative and left derivative is the same at the discontinuity. Hence the L.H.S. and R.H.S. of Eq.(3) diverge identically. This is understood when we note that when $\kappa_2 \rightarrow 0$

$$\frac{2|\tilde{r}_{11}|}{hv_1} \int_{-\infty}^{\infty} dx \cos(2k_1 x + \eta_1) = 0 \quad \text{as} \quad \tilde{r}_{11} = 0$$

The inset shows the behavior of $|\tilde{r}_{11}|^2$ in the entire regime and shows that it goes to 0 at the band edge ($EW^2 = 4\pi^2$, considering $2m_e = 1$ & $\hbar = 1$). The fact that $|\tilde{r}_{11}|^2$ goes to zero at the band edge was analytically shown in [5]. Also it is known that when $\tilde{r}_{11} = 0$ then $\tau_p = 0$ [10] and hence $\hat{\Sigma}^a = 0$. Note that as $\kappa_2 \rightarrow 0$ then $\tilde{r}_{11} = 0$ for all possible choices of width W and impurity strength γ

and hence for all energies. So at the band edge we also have $\frac{\partial \hat{\Sigma}^a}{\partial E} = 0$ and hence the agreement. Fig.(3) shows similar things for a stronger impurity. Fig.(4) considers a negative δ -function potential such that the bound state is below the propagating threshold.

For the negative δ function potential with the bound state in the propagating threshold, we have plotted the two sides of Eq.(3) in Fig.(5). $|\tilde{t}_{11}|^2$ is shown in the inset. Note that $|\tilde{t}_{11}|^2$ shows that at the point P the system is in extreme non-WKB regime where $|\tilde{t}_{11}|^2$ goes to zero. At this energy there is a quasi-bound state. The peak in $\pi[\rho(E) - \rho_0(E)]$ at P occurs due to the quasi-bound state. We also see that at this very point P there is an exact agreement between L.H.S. & R.H.S. of Eq.(3). This can be even verified analytically. Substituting the bound state condition given in Eq.(30) into $\frac{d\theta_f}{dE}$ we get

$$\frac{d\theta_f}{dE} = \frac{m_e k_1}{\hbar^2} \frac{1}{\Gamma_{11}} \sum_{n>1} \frac{\Gamma_{nn}}{\kappa_n^3} \quad (38)$$

and substituting this condition(Eq.(30)) in $\pi[\rho(E) - \rho_0(E)]$ we get

$$\pi[\rho(E) - \rho_0(E)] = \frac{m_e k_1}{\hbar^2} \frac{1}{\Gamma_{11}} \sum_{n>1} \frac{\Gamma_{nn}}{\kappa_n^3} \quad (39)$$

This agreement between $\frac{d\theta_f}{dE}$ and $\pi[\rho(E) - \rho_0(E)]$ was argued to be equal for the case of stub in ref [9] at the transmission zero where the $\frac{\partial \hat{\Sigma}^a}{\partial E}$ term in Eq.(10) and the oscillatory LDOS in Eq.(32) was dropped from the very beginning [9]. Even after including these terms we get exact agreement at the transmission zero for the negative δ function potential in a quantum wire, although the transmission zero is in extreme non-WKB regime. The reasons are as follows. At the transmission zero, since there is a quasi-bound state, $\hat{\Sigma}^a$ becomes minimum and $\frac{\partial \hat{\Sigma}^a}{\partial E} = 0$. Secondly, since the delta function potential is a point impurity, the integrated LDOS in the leads extends from $-\infty$ to ∞ . One can do the integration to find $\int_{-\infty}^{\infty} dx \cos(2k_m x + \eta_m) = \pi \cos(\eta_m) \delta(k_m)$. So the agreement at the energy corresponding to the quasi-bound state will be there unless the quasi-bound state coincides with $k_m = 0$, for then the LDOS in the leads does not integrate to zero. All the arguments are also true for the stub because the stub is also a point scatterer in 1D [15]. However for a scatterer of finite size, the integrated LDOS in the leads will not be zero and one has to depend on screening to set it to zero.

Note that the multichannel case was analyzed in Ref. [7]. When two modes are propagating, the bound state coming from the 3rd sub-band, can be degenerate with the propagating channels. At that point there is no agreement between $\frac{d\theta_f}{dE}$ and $\pi[\rho(E) - \rho_0(E)]$. While $\pi[\rho(E) - \rho_0(E)]$ is not only positive definite, it also has a sharp peak meaning enhanced DOS at the energy corresponding to the bound state. The peak is completely missing from $\frac{d\theta_f}{dE}$ and $\frac{d\theta_f}{dE}$ turns out to be negative. Thus

the disagreement is not just a quantitative one coming from dispersive behaviors, but is a qualitative one.

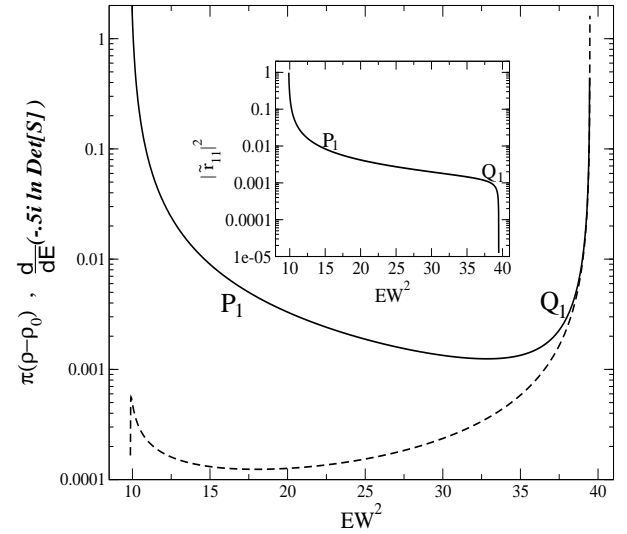


FIG. 2. The system under consideration is shown in Fig. (1). Here we have considered 500 evanescent modes. The dashed curve gives $\pi(\rho - \rho_0)$ and the solid curve gives $\frac{d}{dE}(-.5i \ln \text{Det}[S])$. Both the functions are plotted versus EW^2 using $x_i = 0$, $y_i = .21W$ and $\gamma = 1$ in linear-log scale. In the inset the corresponding $|\tilde{t}_{11}|^2$ is plotted in linear-log scale.

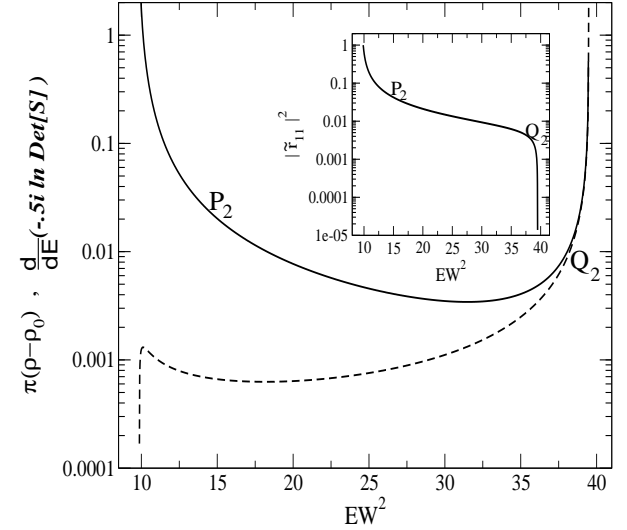


FIG. 3. The system under consideration is shown in Fig. (1). Here we have considered 1000 evanescent modes. The dashed curve gives $\pi(\rho - \rho_0)$ and the solid curve gives $\frac{d}{dE}(-.5i \ln \text{Det}[S])$. Both the functions are plotted versus EW^2 using $x_i = 0$, $y_i = .21W$ and $\gamma = 10$ in linear-log scale. In the inset the corresponding $|\tilde{t}_{11}|^2$ is plotted in linear-log scale.

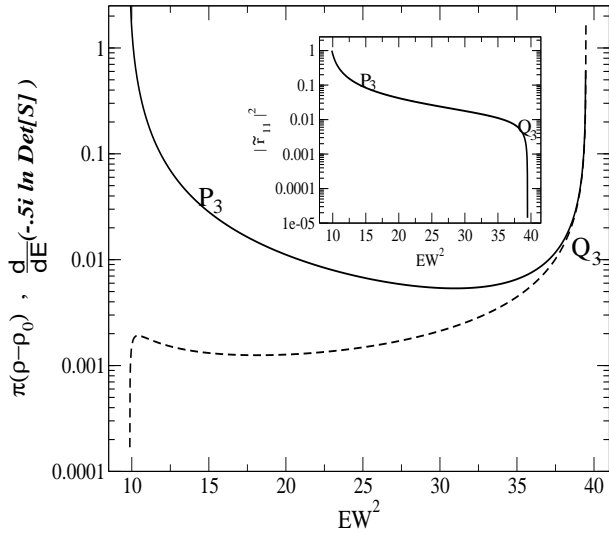


FIG. 4. The system under consideration is shown in Fig. (1). Here we have considered 1000 evanescent modes. The dashed curve gives $\pi(\rho - \rho_0)$ and the solid curve gives $\frac{d}{dE}(-.5i \ln \text{Det}[S])$. Both the functions are plotted versus EW^2 using $x_i = 0$, $y_i = .21W$ and $\gamma = -10$ in linear-log scale. In the inset the corresponding $|\tilde{r}_{11}|^2$ is plotted in linear-log scale.

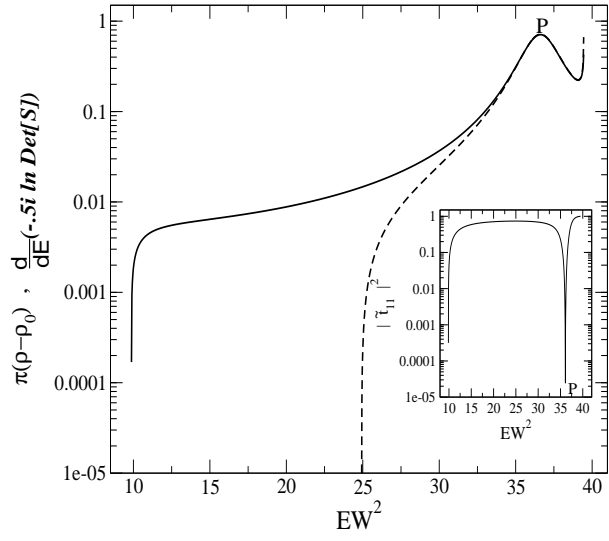


FIG. 5. The system under consideration is shown in Fig. (1). Here we have considered 500 evanescent modes. The solid curve gives $\pi(\rho - \rho_0)$ and the dashed curve gives $\frac{d}{dE}(-.5i \ln \text{Det}[S])$. Both the functions are plotted versus EW^2 using $x_i = 0$, $y_i = .21W$ and $\gamma = -1.5$ in linear-log scale. For this value of γ there is a quasi-bound state at $EW^2 = 36.1022$. In the inset the corresponding $|\tilde{r}_{11}|^2$ is plotted in linear-log scale.

V. CONCLUSION

Thus the Q1D regime behaves very randomly as far as FSR is concerned. Sometimes there is strong agreement in non-WKB regime and sometimes strong disagreement in WKB regime and vice versa. We derive an expression for the DOS, given in Eq.(34) and Eq.(26), that depends on the internal wave functions, but can be estimated exactly from the energy derivative of the S -matrix, at the maxima only in case of a single channel quantum wire. The maxima can be in the WKB regime as well as in the non-WKB regime. This expression (34) and Eq.(26) is basically the integrated change in LDOS, due to the impurity and around the impurity, decaying away from it. It is hence an important physical quantity. The corresponding change in the LDOS in the leads is often unimportant because there the carrier concentration is very high and changes in LDOS are easily screened away. We have shown in our previous work [7] that such a determination of DOS from the energy derivative of S -matrix is not possible for more than one propagating channel.

ACKNOWLEDGMENTS

One of the authors(S.B.) gratefully thanks Prof. Binayak Dutta Roy and Debasish Chaudhuri for useful discussions.

APPENDIX

Here we show the derivation of Eq.(32) for 2 propagating modes. The global density of states is given by

$$\rho(E) = \sum_{m,k_m} \delta(E - E_{m,k_m}) \int_{-\infty}^{\infty} dx \int_{-\frac{W}{2}}^{\frac{W}{2}} dy \sum_{n,k_n} |\psi_{n,k_n}(x, y)|^2 \quad (40)$$

where $\psi_{n,k_n}(x, y) = \sum_n c_n^{(m)}(x) \chi_n(y)$ and E_{m,k_m} is the energy of an electron in the leads.

$E_{m,k_m} = \frac{m^2 \pi^2 \hbar^2}{2m_e W^2} + \frac{\hbar^2 k_m^2}{2m_e}$, where $m = \pm 1, \pm 2$, as there are two propagating modes in the leads.

As $\chi_n(y)$'s form an orthonormal set,

$$\rho(E) = \sum_{m,k_m} \delta(E - E_{m,k_m}) \int_{-\infty}^{\infty} dx \sum_n |c_n^{(m)}(x)|^2$$

First considering electron incident from the left, the partial density of states is

$$\begin{aligned}
\rho_1(E) &= \frac{1}{hv_1} \int_{-\infty}^{\infty} dx \sum_n \left| c_n^{(1)}(x) \right|^2 \\
&+ \frac{1}{hv_2} \int_{-\infty}^{\infty} dx \sum_n \left| c_n^{(2)}(x) \right|^2 \\
&= \frac{1}{hv_1} T1 + \frac{1}{hv_2} T2
\end{aligned} \tag{41}$$

So

$$\rho(E) = \rho_1(E) + \rho_2(E)$$

where $\rho_2(E)$ is the partial DOS for electron incident from the right. Here, $v_1 = \frac{\hbar k_1}{m_e}$ and $v_2 = \frac{\hbar k_2}{m_e}$.

Now,

$$T1 = \int_{-\infty}^{\infty} dx \sum_n \left| c_n^{(1)}(x) \right|^2 \tag{42}$$

where electron is incident in the fundamental mode (denoted by superscript(1)),

$$c_1^{(1)}(x) = \begin{cases} e^{ik_1 x} + \tilde{r}_{11} e^{-ik_1 x} & \text{for } x < 0 \\ \tilde{t}_{11} e^{ik_1 x} & \text{for } x > 0 \end{cases}$$

$$c_2^{(1)}(x) = \begin{cases} \tilde{r}_{12} e^{-ik_2 x} & \text{for } x < 0 \\ \tilde{t}_{12} e^{ik_2 x} & \text{for } x > 0 \end{cases}$$

and for $n > 2$,

$$c_n^{(1)}(x) = \begin{cases} t_{1n} e^{\kappa_n x} & \text{for } x < 0 \\ t_{1n} e^{-\kappa_n x} & \text{for } x > 0 \end{cases}$$

So,

$$\begin{aligned}
T1 &= \int_{-\infty}^0 dx [1 + |\tilde{r}_{11}|^2 + 2|\tilde{r}_{11}| \cos(2k_1 x + \eta_1)] \\
&+ \int_0^{\infty} dx |\tilde{t}_{11}|^2 + \int_{-\infty}^0 dx |\tilde{r}_{12}|^2 + \int_0^{\infty} dx |\tilde{t}_{12}|^2 \\
&+ \frac{|t_{13}|^2}{\kappa_3} + \frac{|t_{14}|^2}{\kappa_4} + \dots
\end{aligned}$$

Here, η_1 is defined as $\tilde{r}_{11} = |\tilde{r}_{11}| e^{-i\eta_1}$.

Similarly, when electron is incident in the 1st excited mode (denoted by superscript(2))

$$\begin{aligned}
T2 &= \int_{-\infty}^{\infty} dx \sum_n \left| c_n^{(2)}(x) \right|^2 \\
&= \int_{-\infty}^0 dx [1 + |\tilde{r}_{22}|^2 + 2|\tilde{r}_{22}| \cos(2k_2 x + \eta_2)] \\
&+ \int_0^{\infty} dx |\tilde{t}_{22}|^2 + \int_{-\infty}^0 dx |\tilde{r}_{21}|^2 + \int_0^{\infty} dx |\tilde{t}_{21}|^2 \\
&+ \frac{|t_{23}|^2}{\kappa_3} + \frac{|t_{24}|^2}{\kappa_3} + \dots
\end{aligned}$$

Here, η_2 is defined as $\tilde{r}_{22} = |\tilde{r}_{22}| e^{-i\eta_2}$.

Therefore,

$$\begin{aligned}
\rho_1(E) &= \frac{1 + |\tilde{r}_{11}|^2}{hv_1} \int_{-\infty}^0 dx + \frac{1 + |\tilde{r}_{22}|^2}{hv_2} \int_{-\infty}^0 dx \\
&+ \frac{|\tilde{r}_{12}|^2}{hv_1} \int_{-\infty}^0 dx + \frac{|\tilde{r}_{21}|^2}{hv_2} \int_{-\infty}^0 dx \\
&+ \frac{2|\tilde{r}_{11}|}{hv_1} \int_{-\infty}^0 dx \cos(2k_1 x + \eta_1) \\
&+ \frac{2|\tilde{r}_{22}|}{hv_2} \int_{-\infty}^0 dx \cos(2k_2 x + \eta_2) \\
&+ \frac{|\tilde{t}_{11}|^2 + |\tilde{t}_{12}|^2}{hv_1} \int_0^{\infty} dx + \frac{|\tilde{t}_{21}|^2 + |\tilde{t}_{22}|^2}{hv_2} \int_0^{\infty} dx \\
&+ \frac{1}{hv_1} \left(\frac{|t_{13}|^2}{\kappa_3} + \frac{|t_{14}|^2}{\kappa_4} + \dots \right) \\
&+ \frac{1}{hv_2} \left(\frac{|t_{23}|^2}{\kappa_3} + \frac{|t_{24}|^2}{\kappa_4} + \dots \right).
\end{aligned}$$

Due to time reversal symmetry, $\tilde{r}_{12} = \tilde{r}_{21}$ & $\tilde{t}_{12} = \tilde{t}_{21}$.

We put $\tilde{r}_{12} = \tilde{r}_{21}$, $\tilde{r}_{21} = \tilde{r}_{12}$, $\tilde{t}_{12} = \tilde{t}_{21}$, $\tilde{t}_{21} = \tilde{t}_{12}$ in the 3rd, 4th, 7th and 8th terms respectively.

Therefore,

$$\begin{aligned}
\rho_1(E) &= \frac{1 + |\tilde{r}_{11}|^2 + |\tilde{r}_{21}|^2}{hv_1} \int_{-\infty}^0 dx \\
&+ \frac{1 + |\tilde{r}_{12}|^2 + |\tilde{r}_{22}|^2}{hv_2} \int_{-\infty}^0 dx \\
&+ \frac{|\tilde{t}_{11}|^2 + |\tilde{t}_{21}|^2}{hv_1} \int_0^{\infty} dx \\
&+ \frac{|\tilde{t}_{12}|^2 + |\tilde{t}_{22}|^2}{hv_2} \int_0^{\infty} dx \\
&+ \frac{2|\tilde{r}_{11}|}{hv_1} \int_{-\infty}^0 dx \cos(2k_1 x + \eta_1) \\
&+ \frac{2|\tilde{r}_{22}|}{hv_2} \int_{-\infty}^0 dx \cos(2k_2 x + \eta_2) \\
&+ \frac{1}{hv_1} \left(\frac{|t_{13}|^2}{\kappa_3} + \frac{|t_{14}|^2}{\kappa_4} + \dots \right) \\
&+ \frac{1}{hv_2} \left(\frac{|t_{23}|^2}{\kappa_3} + \frac{|t_{24}|^2}{\kappa_4} + \dots \right).
\end{aligned}$$

Now adding and subtracting the following terms,

$$\frac{|\tilde{t}_{11}|^2}{hv_1} \int_{-\infty}^0 dx, \frac{|\tilde{t}_{21}|^2}{hv_1} \int_{-\infty}^0 dx, \frac{|\tilde{t}_{22}|^2}{hv_2} \int_{-\infty}^0 dx, \frac{|\tilde{t}_{12}|^2}{hv_2} \int_{-\infty}^0 dx,$$

we get,

$$\begin{aligned}
\rho_1(E) &= \frac{1 + |\tilde{r}_{11}|^2 + |\tilde{r}_{21}|^2 + |\tilde{t}_{11}|^2 + |\tilde{t}_{21}|^2}{hv_1} \int_{-\infty}^0 dx \\
&+ \frac{1 + |\tilde{r}_{12}|^2 + |\tilde{r}_{22}|^2 + |\tilde{t}_{12}|^2 + |\tilde{t}_{22}|^2}{hv_2} \int_{-\infty}^0 dx
\end{aligned}$$

$$\begin{aligned}
& + \frac{2|\tilde{r}_{11}|}{hv_1} \int_{-\infty}^0 dx \cos(2k_1 x + \eta_1) \\
& + \frac{2|\tilde{r}_{22}|}{hv_2} \int_{-\infty}^0 dx \cos(2k_2 x + \eta_2) \\
& + \frac{1}{hv_1} \left(\frac{|t_{13}|^2}{\kappa_3} + \frac{|t_{14}|^2}{\kappa_4} + \dots \right) \\
& + \frac{1}{hv_2} \left(\frac{|t_{23}|^2}{\kappa_3} + \frac{|t_{24}|^2}{\kappa_4} + \dots \right).
\end{aligned}$$

Now $|\tilde{r}_{11}|^2 + |\tilde{r}_{21}|^2 + |\tilde{t}_{11}|^2 + |\tilde{t}_{21}|^2 = 1$ and $|\tilde{r}_{12}|^2 + |\tilde{r}_{22}|^2 + |\tilde{t}_{12}|^2 + |\tilde{t}_{21}|^2 = 1$. Similarly we can calculate $\rho_2(E)$ and thus,

$$\begin{aligned}
\rho(E) = & \frac{2}{hv_1} \int_{-\infty}^{\infty} dx + \frac{2}{hv_2} \int_{-\infty}^{\infty} dx \\
& + \frac{2|\tilde{r}_{11}|}{hv_1} \int_{-\infty}^{\infty} dx \cos(2k_1 x + \eta_1) \\
& + \frac{2|\tilde{r}_{22}|}{hv_2} \int_{-\infty}^{\infty} dx \cos(2k_2 x + \eta_2) \\
& + \frac{2}{hv_1} \left(\frac{|t_{13}|^2}{\kappa_3} + \frac{|t_{14}|^2}{\kappa_4} + \dots \right) \\
& + \frac{2}{hv_2} \left(\frac{|t_{23}|^2}{\kappa_3} + \frac{|t_{24}|^2}{\kappa_4} + \dots \right). \quad (43)
\end{aligned}$$

Now $\frac{2}{hv_1} \int_{-\infty}^{\infty} dx + \frac{2}{hv_2} \int_{-\infty}^{\infty} dx = \rho_0(E)$ i.e. DOS in the absence of scatterer. So we get

$$\begin{aligned}
\rho(E) = & \rho_0(E) + \frac{2|\tilde{r}_{11}|}{hv_1} \int_{-\infty}^{\infty} dx \cos(2k_1 x + \eta_1) \\
& + \frac{2|\tilde{r}_{22}|}{hv_2} \int_{-\infty}^{\infty} dx \cos(2k_2 x + \eta_2) \\
& + \frac{2}{hv_1} \left(\frac{|t_{13}|^2}{\kappa_3} + \frac{|t_{14}|^2}{\kappa_4} + \dots \right) \\
& + \frac{2}{hv_2} \left(\frac{|t_{23}|^2}{\kappa_3} + \frac{|t_{24}|^2}{\kappa_4} + \dots \right).
\end{aligned}$$

[1] M. Büttiker, *Pramana Journal of Physics*, **58**, 241 (2002);
G. Hackenbroich, *Phys. Rep.* **343**, 463 (2001)

[2] J.Friedel, *Philos. Mag.* **43**, 153 (1952); J.M. Ziman, *Principles of the Theory of Solids*.

[3] J.S.Langer and V.Ambegaokar, *Phys. Rev.* **121**, 1090 (1961)

[4] V. Gasperin, T. Christen and M. Büttiker, *Phys. Rev. A* **54**, 4022 (1996).

[5] P.F.Bagwell, *Phys. Rev.B* **41**, 10354(1990)

[6] P. Singha Deo, *Solid State Commun.* **107**, 69 (1998)

[7] P. S. Deo, S. Bandopadhyay and S. Das, *IJMP B*, **16**, 2247 (2002)

[8] H.W.Lee, *Phys. Rev. Lett.* **82**, 2358 (1999)

[9] T.Taniguchi and M.Büttiker, *Phys. Rev.B* **60**, 13814 (1999)

[10] S. Datta, *Electronic Transport in Mesoscopic Systems*. Cambridge University Press, Cambridge, UK, (1997).

[11] J.M.Ziman, *Principles of the Theory of Solids. 2nd ed.* Cambridge University Press, (November 1979)

[12] A.L. Yeyati and M. Büttiker, *PRB*, **62**, 7307 (2000)

[13] E.Merzbacher, *Quantum Mechanics. 3rd ed.* New York : Wiley, (1997)

[14] P. S. Deo and A. M. Jayannavar, *PRB*, **50**, 11629 (1994).
We have also found that if we take two delta function potentials in a single channel quantum wire and place two of them close to each other, then for very large strengths of the two potentials, the system becomes almost reflectionless. This is very counterintuitive as large potentials are expected to give large reflections. It happens because strong potential couples the evanescent modes very strongly to the propagating mode at the positions of the delta potentials, and an incident electron is thrown into the evanescent channels rather than reflected. And since the two potentials are close to each other, the electron can easily tunnel from one potential site to the other and finally go to the transmission channel, again due to the large coupling between the evanescent and transmission channels.

[15] P. S. Deo, *Phys. Rev. B* **53**, 15447(1996)